RESEARCH ARTICLE

3D Printed Zn-doped Mesoporous Silica-incorporated Poly-L-lactic Acid Scaffolds for Bone Repair

Guowen Qian[1], Lemin Zhang[1], Guoyong Wang[1], Zhengyu Zhao[2], Shuping Peng[3,4]*, Cijun Shuai[1,2,5]*

[1]Institute of Bioadditive Manufacturing, Jiangxi University of Science and Technology, Nanchang 330013, China
[2]Shenzhen Institute of Information Technology, Shenzhen 518172, China
[3]NHC Key Laboratory of Carcinogenesis, School of basic Medical Science, Central South University, Changsha, Hunan 410013, China
[4]School of Energy and Machinery Engineering, Jiangxi University of Science and Technology, Nanchang 330013, China
[5]State Key Laboratory of High Performance Complex Manufacturing, Central South University, Changsha 410083, China

Abstract: Poly-L-lactic acid (PLLA) lacks osteogenic activity, which limits its application in bone repair. Zinc (Zn) is widely applied to strengthen the biological properties of polymers due to its excellent osteogenic activity. In the present study, Zn-doped mesoporous silica (Zn-MS) particles were synthesized by one-pot hydrothermal method. Then, the particles were induced into PLLA scaffolds prepared by selective laser sintering technique, aiming to improve their osteogenic activity. Our results showed that the synthesized particles possessed rosette-like morphology and uniform mesoporous structure, and the composite scaffold displayed the sustained release of Zn ion in a low concentration range, which was attributed to the shield effect of the PLLA matrix and the strong bonding interaction of Si-O-Zn. The scaffold could evidently promote osteogenesis differentiation of mouse bone marrow mesenchymal stem cells by upregulating their osteogenesis-related gene expression. Besides, Zn-MS particles could significantly increase the compressive strength of the PLLA scaffold because of their rosette-like morphology and mesoporous structure, which can form micromechanical interlocking with the PLLA matrix. The Zn-MS particles possess great potential to improve various polymer scaffold properties due to their advantageous morphology and physicochemical properties.

Keywords: Poly-L-lactic acid; Zinc doped mesoporous silica; Bone repair

***Correspondence to:** Shuping Peng, School of basic Medical Science, Central South University, Changsha, Hunan 410013, China; shuping@csu.edu.cn; Cijun Shuai, Institute of Bioadditive Manufacturing, Jiangxi University of Science and Technology, Nanchang, Jiangxi 330013, China; shuai@csu.edu.cn

Received: January 13, 2021; **Accepted:** February 15, 2021; **Published Online:** March 10, 2021

Citation: Qian G, Zhang L, Wang G, *et al*., 2021, 3D Printed Zn-doped Mesoporous Silica-incorporated Poly-L-lactic Acid Scaffolds for Bone Repair. *Int J Bioprint,* 7(2):346. http://doi.org/10.18063/ijb.v7i2.346

1 Introduction

Poly-L-lactic acid (PLLA) has attracted great attention in bone repair due to its good biocompatibility and biodegradability[1-4]. PLLA is approved by the U.S. Food and Drug Administration (FDA) for clinical applications. Because the product of PLLA degradation is α-hydroxy acid, which can participate in the carboxylic acid cycle and completely excrete in a physiological environment. However, PLLA lacks osteogenic activity, which limits its application in bone repair.

The amount of Zn in skeleton accounts for 30% of the total amount of Zn in body, which is an essential trace element for skeletal growth[5]. It has been extensively used for bone regeneration due to its ability to improve osteoblast differentiation[6]. In view of this, many Zn alloys were also developed into bone repair materials[7]. Meanwhile, Zn was often acted as an osteogenic active agent and integrated with various polymers, which exhibited great potential in improving biological properties of these polymers[8]. However, the previous studies mainly used ZnO particles as Zn sources[9-11]. In this case, the burst release of Zn ion from ZnO can induce cytotoxicity[12]. In addition, the release of Zn destroys ZnO particles, thus decreasing mechanical properties of the polymers[13].

Mesoporous silica (MS) particles have been widely used in biomedicine, diagnostics, and tissue repair fields due to their good biocompatibility, adjustable morphology, controllable particle size, and mesoporous structure[14-16]. Particularly, MS is also a good vehicle for loading and sustained release of active constituents or functional drugs through mesopores[17]. Meanwhile, MS possesses stable Si-O-Si network structure, which gives the flexibility for doping metal element into MS framework by partial substituting Si sites and forming Si-O-M bond (M=Ca, Mg, and Zn)[18]. The Si-O-Zn bond is more stable than the Zn-O-Zn bond of ZnO, thus guaranteeing the sustained release of Zn ion and its long-term stability.

Ideal artificial bones not only require excellent osteogenic activity but also need to possess three-dimensional (3D) interconnected pore structures for ingrowth of new bone and blood vessel[19-21]. 3D printing technology is a layer-by-layer manufacturing process based on computer model, which can prepare scaffolds with sophisticated shape and internal structure[22]. More encouragingly, bioprinting is able to print personalized live tissues/organs and is expected to achieve the substitute of patient-specific tissues/organs. Selective laser sintering (SLS), as one of the 3D printing techniques, involves powder bed laser fusion additive manufacturing processes[23,24]. SLS exhibits great advantages in the preparation of artificial bones, because there is no need for support materials, binders, or organic solvents during laser forming[25,26]. Meanwhile, it possesses high printing accuracy and material utilization rate.

In the present study, Zn-MS particles were synthesized through one-pot hydrothermal method, and then incorporated into the PLLA scaffold fabricated by SLS technology to improve its osteogenic activities. The morphology, size, mesoporous structure, and compositions of the synthesized Zn-MS particles were analyzed. Meanwhile, the effect of Zn-MS on the hydrophilicity, mechanical properties, ionic release, and cellular behaviors of the PLLA scaffold was systematically evaluated.

2 Materials and methods

2.1 Preparation of Zn-MS

In a typical method, 0.55 g of $Zn(CH_3COO)_2$ (Aladdin, China) and 10 g of N,N-dimethylethanolamine (DMEA, Aladdin, China) were dissolved in 5 mL of ultrapure water. Then, 3.32 g of tetraethyl orthosilicate (TEOS, Aladdin, China) was added. After reacting under an ultrasonic condition at 50°C for 10 min, the gels were then moved to Teflon vessels which were placed in stainless steel autoclaves, and then hydrothermally reacted in an oven at 160°C for 24 h. Afterward, the white precipitates were washed 3 times with ultrapure water and twice with ethanol, and dried at 80°C for 12 h. Finally, the powders were heated at 500°C for 2 h.

2.2 Physicochemical characterization of Zn-MS

Zn-MS particles were observed by a transmission electron microscopy (TEM, JEOL, 2100F, Japan). The microstructure of Zn-MS was analyzed using a scanning electron microscope (SEM, EVO18, ZEISS, Germany). The phases of Zn-MS were determined using an X-ray diffractometry (XRD, DY2472, Malvern PANalytical, Netherlands). The nitrogen adsorption desorption isotherm of Zn-MS was recording using a surface area and porosity analyzer (ASAP2460, Micromeritics, USA). The chemical compositions of Zn-MS were measured using an X-ray photoelectron spectrometer (XPS, Thermo, USA).

2.3 Preparation of Zn-MS/PLLA composite scaffolds

As for the preparation of mixed powders, Zn-MS powders were mixed with PLLA powders by manual grinding for 1 h, and then the mixed powders were added in anhydrous ethanol and were agitated for 4 h under ultrasound condition. After vacuum filtration and dry, the mixed powders were collected for laser forming. Zn-MS/PLLA composite scaffolds were prepared by self-developed SLS system. Specifically, the mixed powders were uniformly spread on the platform, and the laser beam selectively melts powders according to the designed pattern. After finishing one layer, the platform moved down based on the designed layer thickness, and then the powders were spread on the platform again before melting by laser beam; finally, the scaffolds were prepared after layer-by-layer melting. During the process of laser forming, the laser power, scanning speed, spot diameter, scanning line space, powder bed temperature, and powder layer thickness were set to 2.4 W, 200 mm/s, 580 μm, 0.8 mm, 20°C, and 0.2 mm, respectively. The composite scaffolds prepared with 2 wt.%, 4 wt.%, and 6 wt.% Zn-MS (with respect to total weight of Zn-MS and PLLA powders) were abbreviated as 2Zn-MS/PLLA, 4Zn-MS/PLLA, and 6Zn-MS/PLLA.

2.4 Characterization of Zn-MS/PLLA composite scaffolds

The photos of Zn-MS/PLLA composite scaffolds were took by a digital camera. The tensile fracture surfaces of the composite scaffolds were observed by SEM equipped with an energy dispersive spectrometer (EDS). The hydrophilic property of the composite scaffolds was measured using a surface contact angle analyzer (DSA100, KRUSS, Germany). The compressive strengths and stress-strain curves of the composite

scaffolds were determined by a universal testing machine (E44.304, Mattes Industrial Systems Co., LTD, China). The hardness of the composite scaffolds was measured using a microhardness tester (TMVS-2, Beijing Time High Technology Co., LTD, China).

2.5 Ions release

The composite scaffolds were immersed into phosphate buffer saline (PBS) for 14 days. The immersion solution was changed with fresh PBS every other day. The changed liquids were collected by centrifugation, and then the Zn and Si ions concentrations in the liquids were measured using an inductively coupled plasma atomic emission spectrometer (ICP-AES, Optima 5300DV, PerkinElmer, USA).

2.6 Cell experiments

(1) Cell adhesion

The PLLA and 4Zn-MS/PLLA samples (Φ6 mm × 2 mm) were fabricated using SLS technique. The samples were sterilized by immersing them in the 70% ethanol solutions overnight and washed 3 times with aseptic PBS. MG-63 osteoblast-like cells were seeded on the PLLA and 4Zn-MS/PLLA samples, and cultured with Dulbecco's modified Eagle medium (DMEM, Gibco) supplied with 10% fetal bovine serum (FBS, Gibco). The culture environment was at 37°C with 5% CO_2. The medium was changed every other day. When the culture time reached 1, 4, and 7 days, the samples containing cells were fixed using 4 vol.% formaldehyde solution. Then, the samples were dehydrated using gradient alcohol solutions. After dehydration, the samples were gold-sprayed and observed by SEM (EVO18, ZEISS, Germany).

(2) Osteogenic-related gene expressions

The mouse bone mesenchymal stem cells (mBMSCs) were cultured on the sterilized samples (Φ10 mm × 2 mm) for 7 and 14 days. Total ribonucleic acid (RNA) was extracted from mBMSCs grew on the samples using column extraction method. Then, complementary deoxyribonucleic acid (cDNA) was synthesized using PrimeScript 1st Strand cDNA Synthesis kits (TakaRa Bio Inc., Kyoto, Japan). Osteogenic-related gene expressions of Runt-related transcription factor 2 (RUNX2), collagen I (COL-I), osteocalcin (OCN), and osteopontin (OPN) were determined using a real-time quantitative fluorescence polymerase chain reaction (RT-PCR) instrument. The expressions of osteoblast-related genes were assayed and normalized in comparison to that of house-keeping gene.

2.7 Statistical analysis

All experiment groups were set at least three parallel samples. All data were indicated as mean ± standard deviation (SD) and analyzed using Student's *t*-test. $p < 0.05$ was deemed to be statistically significant.

3 Results and discussions

3.1 Synthesis and characterization of Zn-MS

Zn-MS particles were synthesized through one-pot hydrothermal method using DMEA as template. As shown in **Figure 1A**, DMEA played structure-guiding and pH-adjusting roles during the synthesis of Zn-MS particles[27]. In detail, DMEA could coordinate with Zn to form $Zn(DMEA)^{2+}$ templates[17]. The $Zn(DMEA)^{2+}$ templates guided the growth of silica into petal-like structure. Then Zn-doped silica petals self-assembled in rosette-like particles during the hydrothermal reaction. In addition, DMEA was a weak base which provided a mildly alkaline environment in the reaction solution, thus leading to slow hydrolysis of TEOS. Therefore, bits of crystal nuclei were generated at the beginning. Then, the nuclei gradually grew as the hydrolysis proceeded. Finally, mesopores on the petals generated after the decomposition of DMEA in the process of heat treatment.

The morphology of Zn-MS is depicted in **Figure 1B**. It can be seen that Zn-MS was stacked by many petal-like nanosheets, and their thickness was about 100 nm. The whole Zn-MS particle displayed rosette-like morphology with average size of 2.5 μm. The average size of interstices between petals was 150 nm. Well-ordered mesoporous structure was observed on the petals, as shown in **Figure 1C and D**. The average mesoporous size on the petals was 3 nm. The dark-field image of Zn-MS was first captured to ensure element analysis at the same exact location (**Figure 1E**). The constituent elements of Zn-MS, that is, Zn, Si, and O, were evenly distributed on the particle surface, as displayed in **Figure 1F-I**. This element mapping results verified that Zn was successfully incorporated into MS.

The X-ray diffraction (XRD) result of Zn-MS is exhibited in **Figure 2A**. The bread-like diffraction peak at 15° – 40° showed that the synthesized Zn-MS particles were amorphous. The synthesized particles had mesopores verified by the existence of an obvious hysteresis loop in the nitrogen adsorption-desorption isotherm (**Figure 2B**). The specific surface area of Zn-MS was about 37.45 m^2/g. The average pore diameter of Zn-MS was about 4.29 nm, which was calculated from the Barrett-Joyner-Halend method. To further prove the incorporation of Zn into MS, XPS analysis was used. Different elements using XPS spectrometer were identified by the Avantage software. The peaks at 1045, 1022, 532, 154, and 103 eV were ascribed to Zn2p1/2, Zn2p3/2, O1s, Si2s, and Si2p, respectively. As shown in **Figure 2C and D**, the Zn-MS particles were consisted of Zn, Si, and O elements. In the Zn 2p spectrum, the peaks

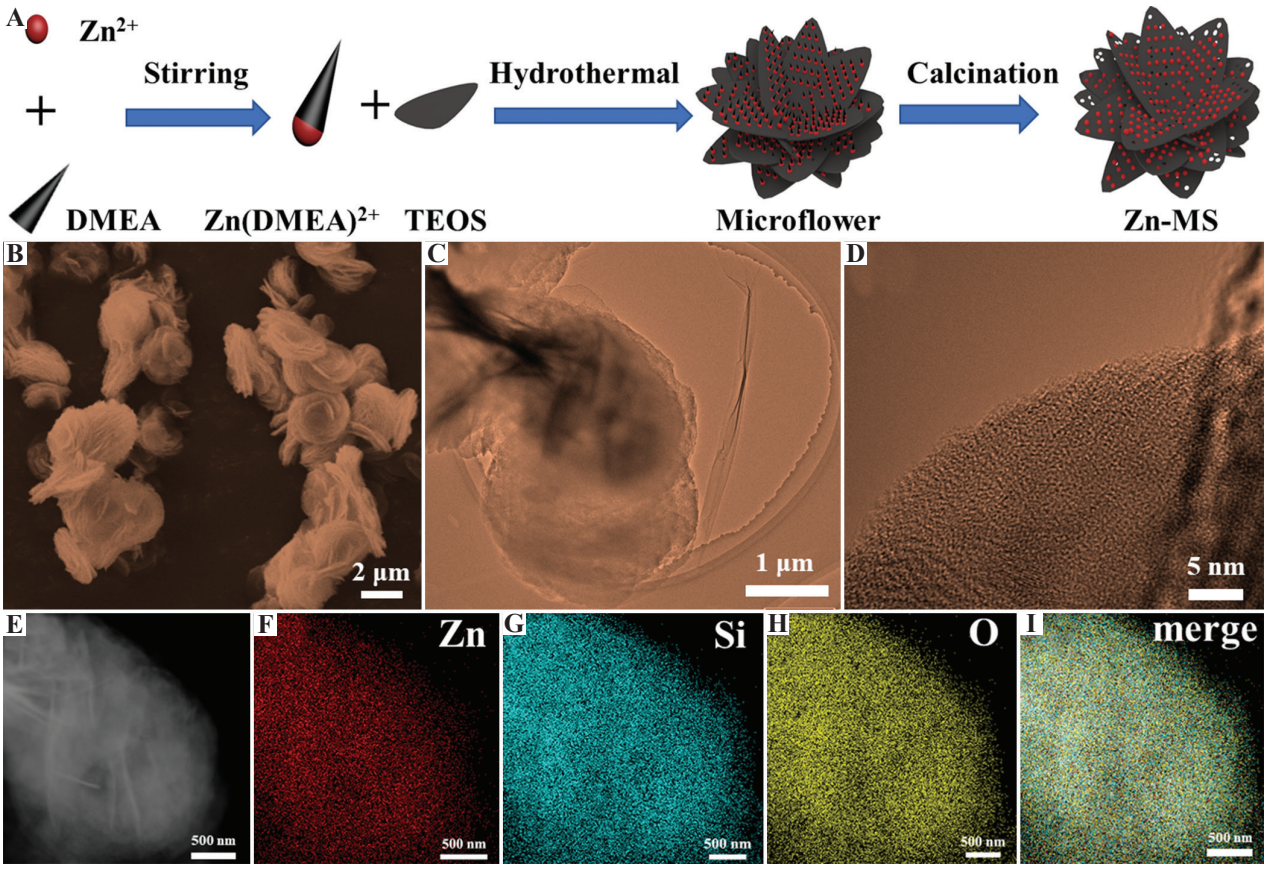

Figure 1. (A) Schematic diagram of the synthesis of zinc-doped mesoporous silica (Zn-MS) particles. **(B)** Images of scanning electron microscope, **(C-D)** transmission electron microscopy, E dark-field, **(F-H)** element distributions and corresponding merge photo **(I)** of the synthesized Zn-MS particles.

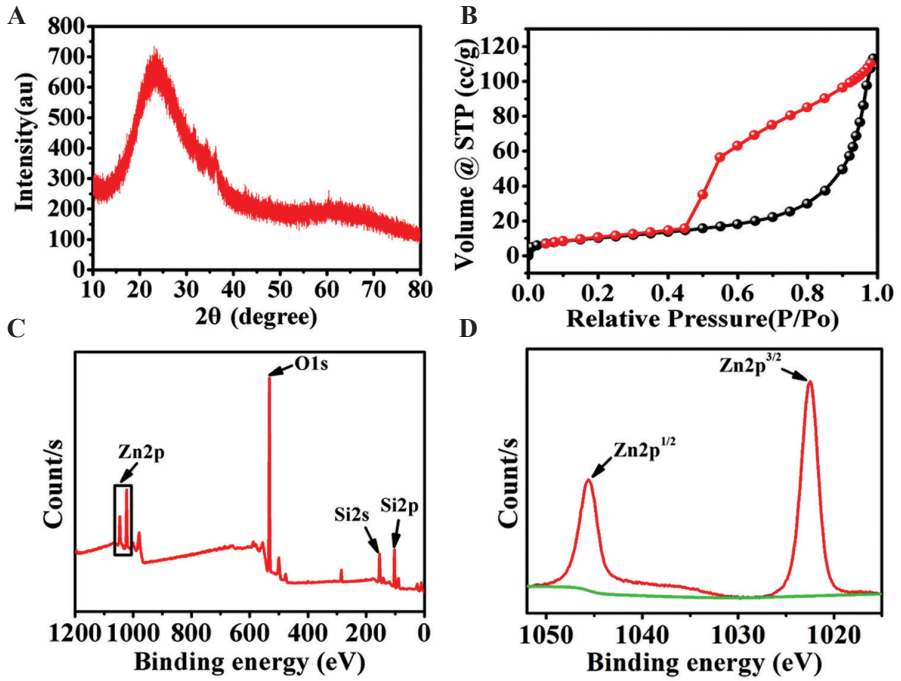

Figure 2. (A) XRD pattern, **(B)** nitrogen adsorption-desorption isotherm, and **(C-D)** XPS spectra of the synthesized Zn-MS particles.

at 1045 and 1022 eV were attributed to the Zn 2p1/2 and Zn 2p3/2 peaks, indicating that Zn ions were successfully doped in the MS.

3.2 Preparation and characterization of composite scaffolds

PLLA was extensively used as bone repair materials due to its excellent biocompatibility, biodegradability, and machinability. However, low osteogenic activity limits its further application in clinical setting. In this study, the synthesized Zn-MS particles were introduced into PLLA to improve these drawbacks due to their ability to release bioactive Zn and Si ions. Meanwhile, ideal bone repair materials also need 3D interconnected porous structure for new bone formation and angiogenesis. SLS technique as an additive manufacturing technology not only can precisely control the pore size, pore shape, and interconnectivity of scaffolds but also can customize personalized shape. Therefore, SLS technique was used to prepare the PLLA composite scaffolds with different amount of Zn-MS. The diameter of fabricated-scaffolds was 12 mm, and their height was 4 mm. As displayed in **Figure 3A**, the scaffolds had regular shape and 3D interconnected pores. The average size of open pores was 650 μm in the printing plane and 250 μm in the vertical direction. Many studies have shown that the 3D porous scaffolds could effectively guide the ingrowth of bone-related cells and new vessels.

The forming quality of the Zn-MS/PLLA scaffolds is closely associated with the dispersion of Zn-MS particles. Aggregation of Zn-MS particles in the matrix can profoundly affect solute diffusion of PLLA melts and densification of the scaffolds, which decreases mechanical properties of the Zn-MS/PLLA scaffolds. To achieve homogeneous dispersion of Zn-MS particles, a series of complicated processes for preparing Zn-MS and PLLA mixed powders, included grinding, ultrasound agitation and vacuum filtration, were performed. The particle distribution on the tensile brittle fracture surface of the composite scaffolds was observed using SEM. As exhibited in **Figure 3B**, the surface of the PLLA scaffold

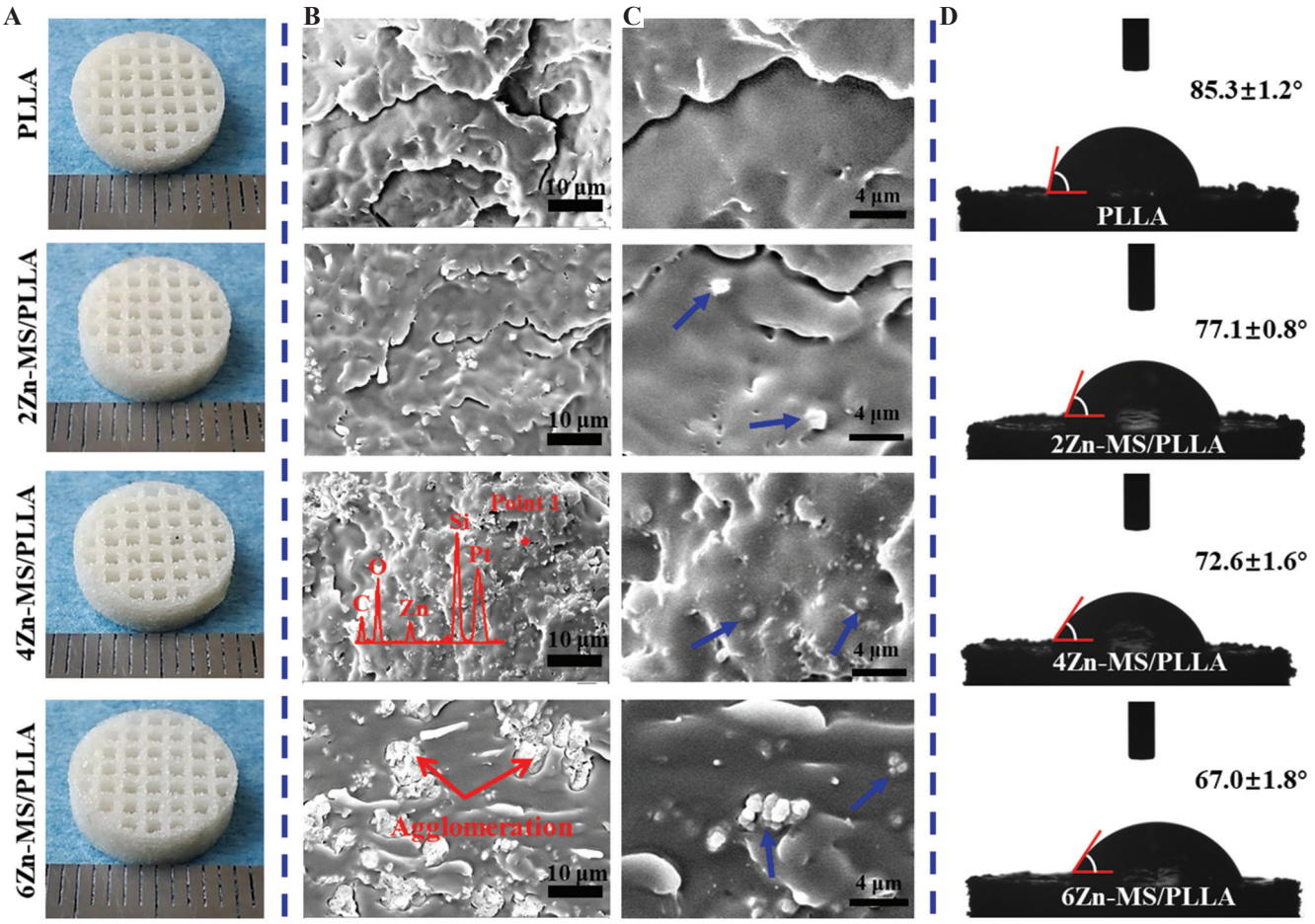

Figure 3. (A) Digital images of the Poly-L-lactic acid scaffolds with different amount of zinc-doped mesoporous silica prepared by selective laser sintering. **(B and C)** Scanning electron microscope images of the tensile brittle fracture surface of the composite scaffolds (point 1 analyzed by energy dispersive spectrometer and particles indicated blue arrows). **(D)** Results of water contact angle of the composite scaffolds.

without Zn-MS was smooth, while many particles were observed on the fractured surface of the composite scaffold with addition of Zn-MS. Moreover, the number of particles increased with increasing amount of Zn-MS. The EDS results confirmed that the components of the particles were Zn, Si, and O elements, indicating the particles were Zn-MS. It was noted that the particles distributed evenly on the PLLA matrix when the adding amount of Zn-MS was below 6 wt.%. However, when the amount of Zn-MS was 6 wt.%, obvious aggregation appeared on the fractured surface of the composite scaffold. As shown in **Figure 3C**, PLLA melts penetrated into the interstices between petals of the rosette-like particles in the process of laser forming, displaying good interfacial bonding between Zn-MS and PLLA. However, Zn-MS particles did not melt and still kept their initial morphology and structure.

The effect of Zn-MS on the hydrophilicity of the PLLA was investigated using a water contact angle meter. As shown in **Figure 3D**, the water contact angle of the PLLA displayed a gradual descending trend with increasing amount of Zn-MS, suggesting Zn-MS evidently enhanced the hydrophilicity of the PLLA. The cellular adhesion ability on the surface of synthesized polymers is dependent on their chemistry properties, such as hydrophilicity, roughness, electronegativity, and others[28-31]. In general, cells cannot adhere on the surface of synthesized-polymers directly because the integrins on the surface of cell membrane can only interact with specific amino acid sequences of proteins in the extracellular matrix[32]. Good hydrophilicity is beneficial to absorb nutrients and proteins in the body fluids, thus significantly promoting cell adhesion[33].

The mechanical properties also collectively represent an important evaluation index for bone repairing materials. The proper mechanical properties of implants are able to reduce the appearance of fracture remarkably and avoid stress-shielding effect[34,35]. The compressive stress-strain curves, compressive strength, compressive modulus, and micro-hardness of the composite scaffolds are exhibited in **Figure 4A-D**. With the increase of Zn-MS amount, the compressive strength and hardness of the composite scaffolds increased first, and then decreased. When the added amount of Zn-MS was 4 wt.%, the compressive strength and hardness of the composite scaffolds were the highest. The average compressive strength of 4Zn-MS/PLLA scaffolds was 10.7 MPa, which surpassed the compressive strength of native cancellous bone (7 – 10 Mpa)[36]. The average compressive modulus of PLLA scaffold without Zn-MS was 131 MPa. When the content of Zn-MS was 4 wt.%, the compressive modulus of the composite scaffold was 294 Mpa. The

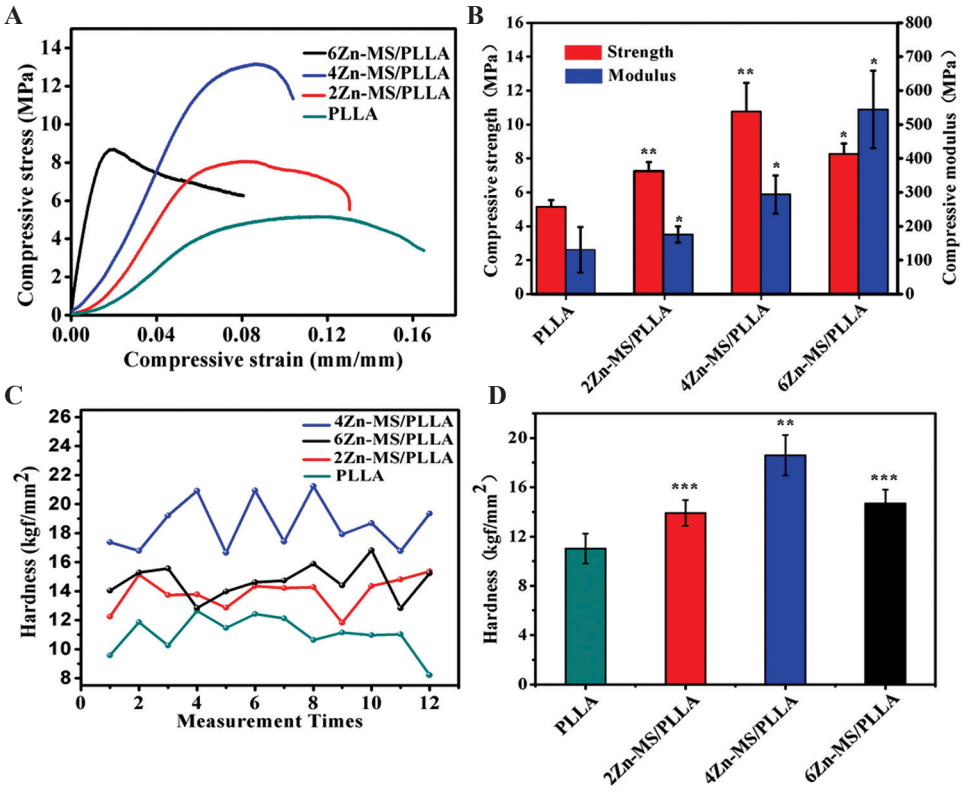

Figure 4. (A) Compressive stress-strain curves, **(B)** compressive strength, **(C-D)** compressive modulus and micro-hardness of the composite scaffolds.

modulus of native cancellous bones was in the range of 50 – 500 MPa[36]. It could be seen that the modulus of the composite scaffold was close to that of native cancellous bone. The probable reasons for strengthening were mainly attributed to two aspects. On the one hand, appropriate amount of Zn-MS evenly distributed in the PLLA matrix, which played a dispersion-strengthening effect[35]. On the other hand, rosette-like morphology and mesoporous structure of Zn-MS were beneficial to the penetration of the PLLA melts into the interstices between petals and mesopores on the petals, thus forming micromechanical interlocking effect[13,37]. However, excessive Zn-MS in the PLLA matrix had an adverse effect on the laser sintering property, thus generating more defects and decreasing compactness of the composite scaffolds, which reduced their mechanical properties[38,39].

Zn ions play an important role in the key enzymes related activity with bone metabolism, mainly including alkaline phosphatase, collagenase, and carbonic anhydrase[40]. Meanwhile, they also directly participated in the metabolism of bone-related cells[41]. In addition, Zn ions also could promote adhesion, spread, proliferation, and osteogenic differentiation of stem cells[42]. However, high concentration of Zn ions can induce cytotoxicity and cell apoptosis[43]. Therefore, the release of Zn from biomaterials needs to be precisely controlled, thus ensuring their biosafety and osteogenesis. The concentrations of Zn released from the composite scaffolds were determined using ICP-AES. As exhibited in **Figure 5A**, the cumulative release concentration of Zn ions for all samples increased with prolonging soaking time. The cumulative release concentration of Zn ions also enhanced with increasing amount of Zn-MS. The Zn release rates for the 4Zn-MS/PLLA and 6Zn-MS/PLLA samples were relatively high at the beginning of immersion (<6 days), then reached a steady phase during the rest of the time. After soaking for 14 days, the cumulative release concentrations of Zn ions for 2Zn-MS/PLLA, 4Zn-MS/PLLA, and 6Zn-MS/PLLA samples were 1.25, 1.76, and 2.36 mg/L. Meanwhile, the average release concentrations of Zn ions during 2 days for the 4Zn-MS/PLLA and 6Zn-MS/PLLA samples gradually decreased at the initial stage (<6 days), and then reached stability, suggesting that the composite scaffolds containing different amount of Zn-MS could achieve sustained release of Zn ions (**Figure 5B**). The probable reasons for sustained release of Zn ions were the shield effect of the PLLA matrix under Van der Waals forces and strong bonding of Si-O-Zn[18,44,45]. When the soaking time was between 12 and 14 days, the average concentrations of Zn ion released from 2Zn-MS/PLLA, 4Zn-MS/PLLA and 6Zn-MS/PLLA were 0.15, 0.18, and 0.21 mg/L, respectively.

The variation of cumulative release concentration of Si ions for different composite scaffolds after being soaked in PBS is exhibited in **Figure 5C**. The Si ion

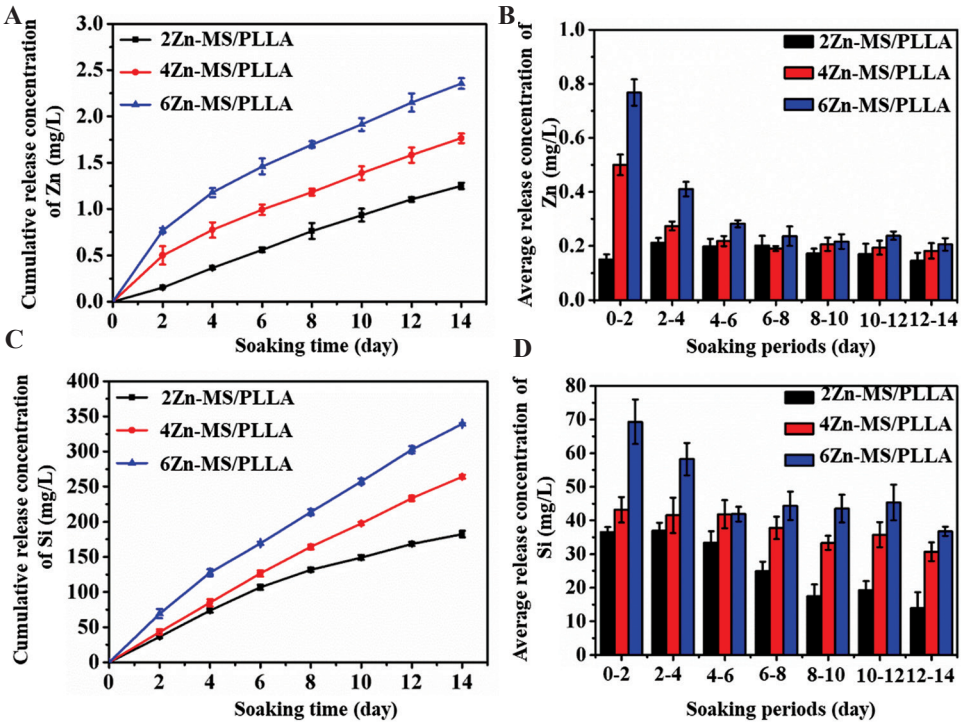

Figure 5. The cumulative release concentration **(A, C)** and the average release concentration **(B, D)** of Zn **(A, B)** and Si **(C, D)** ions of the poly-L-lactic acid composite scaffolds with different amount of zinc-doped mesoporous silica after soaking in phosphate buffer saline for different times.

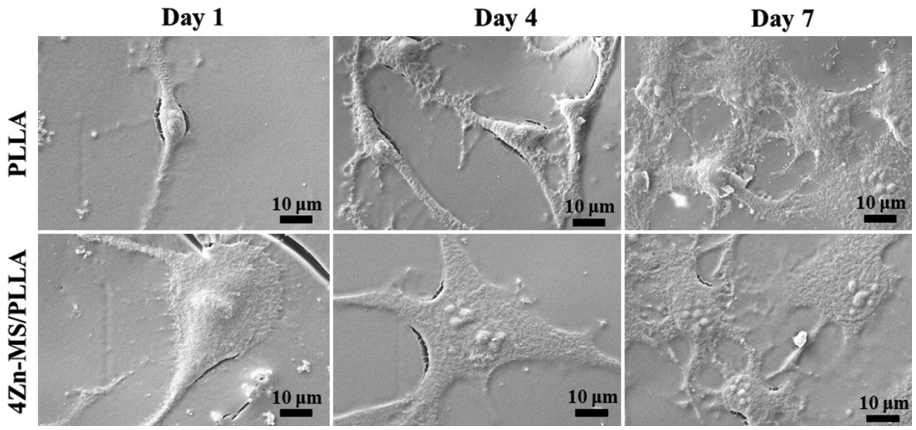

Figure 6. The morphology of osteoblast-like MG-63 cells grew on the poly-L-lactic acid (PLLA) and 4 zinc-doped mesoporous silica/PLLA samples after cultured for 1, 4, and 7 days.

cumulative release concentrations for all composite scaffolds increased with the prolongation of soaking time. Meanwhile, the Si ion cumulative release concentrations enhanced with increasing the contents of Zn-MS. After soaking for 14 days, the cumulative release concentrations of Si ions were 182.58, 264.09, and 339.33 mg/L, respectively. The average Si ion release concentrations for different composite scaffolds during 2 days are displayed in **Figure 5D**. The average Si ion release concentration for the 2Zn-MS/PLLA scaffold decreased with the prolongation of soaking time. In the case of 4Zn-MS/PLLA and 6Zn-MS/PLLA scaffolds, the average Si ion release concentration decreased first, and then tended to stabilize (**Figure 5D**). When the soaking time was between 12 and 14 days, the average Si ion release concentrations for the 2Zn-MS/PLLA, 4Zn-MS/PLLA, and 6Zn-MS/PLLA composite scaffolds were 14.01, 30.71, and 36.75 mg/L, respectively.

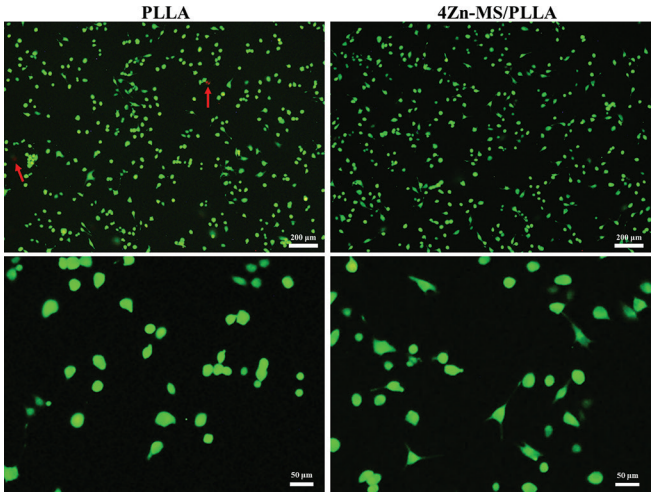

Figure 7. Live-dead fluorescence staining images of MG-63 cells after cultured on the poly-L-lactic acid (PLLA) and 4 zinc-doped mesoporous silica/PLLA scaffold for 1 day (dead cells indicated by red arrows).

3.3 Cellular behaviors of composite scaffolds

According to the results of mechanical properties, the 4Zn-MS/PLLA sample was selected to evaluate the effect of Zn-MS on cellular behaviors. The spread morphology of osteoblast-like MG-63 cells on the PLLA and 4Zn-MS/PLLA samples after cultured for 1, 4, and 7 days is shown in **Figure 6**. The spread area of MG-63 cells grew on the 4Zn-MS/PLLA was larger than that grew on the PLLA, and the adhesion between cell and matrix for the 4Zn-MS/PLLA sample was tighter than that for the PLLA sample. Moreover, the cells grew on the 4Zn-MS/PLLA sample exhibited more pseudopods in comparison to that on the PLLA sample, suggesting that Zn-MS evidently promoted cell adhesion and spread.

The live-dead fluorescence staining images are shown in **Figure 7**. Meanwhile, green fluorescence indicates live cell, while red fluorescence denotes dead cell. It could be seen that almost no dead cells were observed on the PLLA and 4Zn-MS/PLLA scaffolds, indicating that both scaffolds had good cytocompatibility. In addition, more cells cultured on the 4Zn-MS/PLLA scaffold displayed obvious filopodia compared to that on the PLLA scaffold, which also showed that Zn-MS could promote cell adhesion. Good adhesion and spread of MG-63 cells on the 4Zn-MS/PLLA were probably attributed to the improved hydrophilicity and sustainedly released active Zn and Si ions.

Stem cells are primitive cells with the potential of self-renewal and multidirectional differentiation, and they are the origin cells of various tissues and organs. The ability to osteogenic differentiation of stem cells stimulated by implants may serve as an important judgment criterion to evaluate their osteogenic activity. Therefore, mBMSCs were co-cultured with the PLLA and 4Zn-MS/PLLA samples, and the expression of bone-related genes of mBMSCs was detected using RT-PCR. The detailed results are showed in **Figure 8**. After cultured for 7 days, Zn-MS obviously upregulated the

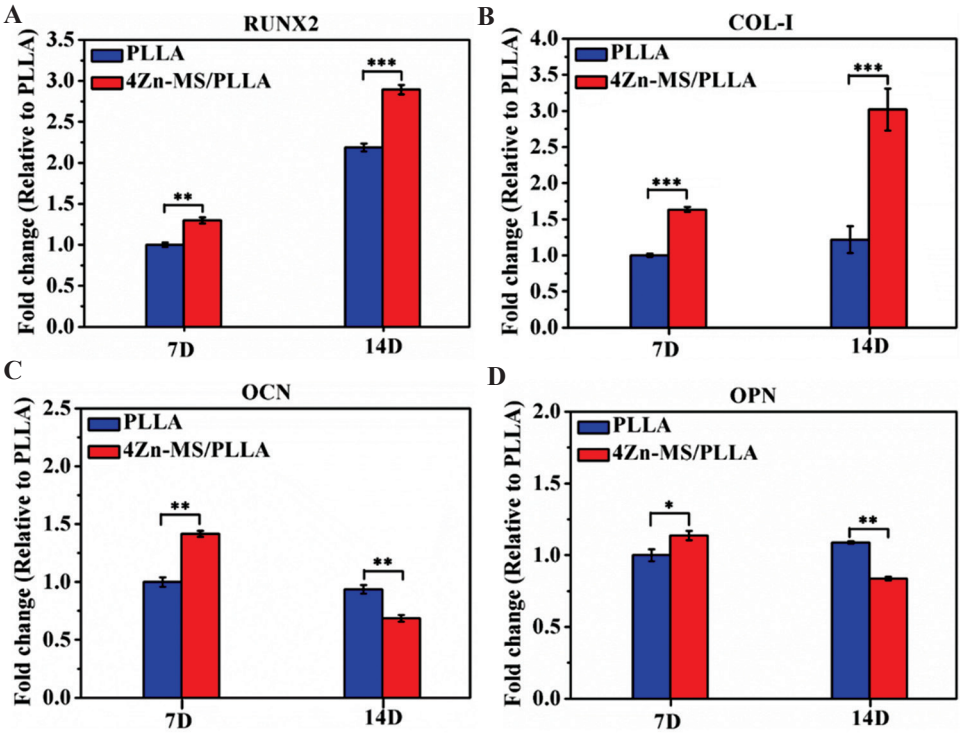

Figure 8. The expression of osteogenesis-related genes of mBMSCs grown on the poly-Llactic acid (PLLA) and 4 zinc-doped mesoporous silica/PLLA scaffolds after being cultured for 7 and 14 days.

expression of RUNX2, COL-I, OCN, and OPN. With an increase of culture time to 14 days, the expression of RUNX2 and COL-I genes was further upregulated, and the expression of RUNX2 and COL-I genes of mBMSCs grown on the 4Zn-MS/PLLA sample was higher than that on the PLLA scaffold. These results showed that Zn-MS particles significantly improved the osteogenic activity of PLLA scaffold.

Many studies demonstrated that Zn ions displayed promoting effects on osteogenesis. The proper Zn ion concentration could improve the adhesion and spread of stem cells by upregulating the expression of integrin. Meanwhile, Zn ions also penetrate into cytoplasm by zinc (Zn) transporter (ZIP1 and ZnT1), thus moderately increasing concentration of intracellular Zn ions. The enhancement of Zn ion concentration in cells further activates MAPK/ERK signaling pathway and upregulates the expression of osteogenesis-related genes. However, high Zn ion concentration (15 mg/L) leads to over-expression of Zn transporter, which makes excessive Zn ions inflow into cytoplasm. And then, the production of reactive oxygen species (ROS) increases, thereby resulting in cell apoptosis[46]. In addition, Si ions are also essential to bone growth[47]. It was reported that Si ions significantly improved the proliferation and osteogenic differentiation of stem cells with involvement of WNT and SHH signaling pathway. However, high Si ion concentration (140 mg/L) could suppress the proliferation of stem cells[48]. In this study, the 4Zn-MS/PLLA composite scaffold sustainedly released Zn ions in a low range (0.18 – 0.5 mg/L) and Si ions in a moderate range (31 – 43 mg/L), reducing the potential cytotoxicity of these metal ions. Therefore, the synthesized Zn-MS particles could effectively improve osteogenic activity of the PLLA scaffold.

4 Conclusions

MS particles (Zn-MS) with rosette-like morphology and uniform mesoporous structure were successfully synthesized by one-pot hydrothermal method. Then, the PLLA composite scaffolds with different amount of Zn-MS were prepared by SLS technique. All composite scaffolds were able to sustainedly release Zn and Si ions. The addition of 4 wt.% Zn-MS not only evidently increased the compressive strength of the PLLA scaffold but also obviously improved the osteogenic activity of the PLLA scaffold. Considering their favorable morphology and sustainedly release active ions, the Zn-MS particles showed tremendous potential to improve mechanical properties and osteogenic activity of various polymer scaffolds.

Acknowledgments

This study was supported by the following funds: (1) The Natural Science Foundation of China (51935014,

82072084, 81871498); (2) JiangXi Provincial Natural Science Foundation of China (20192ACB20005, 2020ACB214004, 20202BAB214011); (3) The Provincial Key R & D Projects of Jiangxi (20201BBE51012); (4) Guangdong Province Higher Vocational Colleges & Schools Pearl River Scholar Funded Scheme (2018); (5) The Project of Hunan Provincial Science and Technology Plan (2017RS3008); (6) Shenzhen Science and Technology Plan Project(JCYJ20170817112445033); (7) Innovation Team Project on University of Guangdong Province(2018GKCXTD001); (8) Technology Innovation Platform Project of Shenzhen Institute of Information Technology 2020 (PT2020E002); (9) High-level Talents Scientific Research Initiation Project of Jiangxi University of Science and Technology (205200100487).

Conflict of interest

The authors declare no conflicts of interest.

Author contributions

G.Q. and L.Z. designed the overall experimental plan and performed experiments. G.Q. and L.Z. interpreted data and wrote the manuscript with support from G.W., Z.Z., S.P. and C.S. C.S. supervised the project and conceived the original idea. All authors read and approved the manuscript.

References

1. Wang G, Qian G, Zan J, *et al*., 2020, A Co-dispersion Nanosystem of Graphene Oxide@ Silicon-doped Hydroxyapatite to Improve Scaffold Properties. *Mater Design*, 2020:109399. https://doi.org/10.1016/j.matdes.2020.109399
2. Shuai C, Yu L, Feng P, *et al*., 2020, Organic Montmorillonite Produced an Interlayer Locking Effect in a Polymer Scaffold to Enhance Interfacial Bonding. *Mater Chem Front*, 4:2398–408. https://doi.org/10.1039/d0qm00254b
3. Shuai C, Yang W, Feng P, *et al*., 2020, Accelerated Degradation of HAP/PLLA Bone Scaffold by PGA Blending Facilitates Bioactivity and Osteoconductivity. *Bioact Mater*, 6:490–502. https://doi.org/10.1016/j.bioactmat.2020.09.001
4. Qi F, Wang C, Peng S, *et al*., 2021, A Co-dispersed Nanosystem from Strontium-Anchored Reduced Graphene Oxide to Enhance Bioactivity and Mechanical Property in Polymer Scaffolds. *Mater Chem Front*, 2021:958. https://doi.org/10.1039/d0qm00958j
5. King JC, Shames DM, Woodhouse LR, 2020, Zinc Homeostasis in Humans. *J Nutr*, 130:1360S–6S.
6. Hadley KB, Newman SM, Hunt JR, 2010, Dietary Zinc Reduces Osteoclast Resorption Activities and Increases Markers of Osteoblast Differentiation, Matrix Maturation, and Mineralization in the Long Bones of Growing Rats. *J Nutr Biochem*, 21:297–303. https://doi.org/10.1016/j.jnutbio.2009.01.002
7. Vojtěch D, Kubásek J, Šerák J, *et al*., 2011, Mechanical and Corrosion Properties of Newly Developed Biodegradable Zn-based Alloys for Bone Fixation. *Acta Biomater*, 7:3515–22. https://doi.org/10.1016/j.actbio.2011.05.008
8. Bejarano J, Boccaccini AR, Covarrubias C, *et al*., 2020, Effect of Cu-and Zn-Doped Bioactive Glasses on the *In Vitro* Bioactivity, Mechanical and Degradation Behavior of Biodegradable PDLLA Scaffolds. *Materials*, 13:2908. https://doi.org/10.3390/ma13132908
9. Harikrishnan P, Sivasamy A, 2020, Preparation, Characterization of Electrospun Polycaprolactone-nano Zinc Oxide Composite Scaffolds for Osteogenic Applications. *Nanostruct Nanoobjects*, 23:100518. https://doi.org/10.1016/j.nanoso.2020.100518
10. Shuai C, Wang C, Qi F, *et al*., 2020, Enhanced Crystallinity and Antibacterial of PHBV Scaffolds Incorporated with Zinc Oxide. *J Nanomater*, 2020:6014816.
11. Xia Y, Fan X, Yang H, *et al*., 2020, ZnO/Nanocarbons-modified Fibrous Scaffolds for Stem Cell-based Osteogenic Differentiation. *Small*, 16:2003010. https://doi.org/10.1002/smll.202003010
12. Wu J, Wang L, He J, *et al*., 2012, *In Vitro* Cytotoxicity of Cu^{2+}, Zn^{2+}, Ag^{+} and their Mixtures on Primary Human Endometrial Epithelial Cells. *Contraception*, 85:509–18. https://doi.org/10.1016/j.contraception.2011.09.016
13. Bai X, Lin C, Wang Y, *et al*., 2020, Preparation of Zn Doped Mesoporous Silica Nanoparticles (Zn-MSNs) for the Improvement of Mechanical and Antibacterial Properties of Dental Resin Composites. *Dent Mater*, 36:794–807. https://doi.org/10.1016/j.dental.2020.03.026
14. Szewczyk A, Skwira A, Ginter M, *et al*., 2021, Microwave-assisted Fabrication of Mesoporous Silica-calcium Phosphate Composites for Dental Application. *Polymers*, 13:53. https://doi.org/10.3390/polym13010053
15. Li X, Wang X, Qian G, *et al*., 2019, Synergistical Chemotherapy and Cancer Immunotherapy Using Dual Drug-delivering and Immunopotentiating Mesoporous Silica. *Appl Mater Today*, 16:102–11. https://doi.org/10.1016/j.apmt.2019.05.006
16. Li X, Shenashen MA, Wang X, *et al*., 2018, Mesoporous Caged-γ-AlOOH-Double-stranded RNA Analog Complexes

for Cancer Immunotherapy. *Adv Biosyst*, 2:1700114. https://doi.org/10.1002/adbi.201700114

17. Qian G, Wang X, Li X, *et al*., 2019, An Immuno-potentiating Vehicle Made of Mesoporous Silica-zinc Oxide Micro-rosettes with Enhanced Doxorubicin Loading for Combined Chemoimmunotherapy. *Chem Commun*, 55:961–4. https://doi.org/10.1039/c8cc09044k
18. Wang X, Li X, Ito A, *et al*., 2017, Biodegradable Metal Ion-doped Mesoporous Silica Nanospheres Stimulate Anticancer Th1 Immune Response *In Vivo*. *ACS Appl Mater Interf*, 9:43538–44. https://doi.org/10.1021/acsami.7b16118.s001
19. Shuai C, Li S, Peng S, *et al*., 2020, Hydrolytic expansion induces corrosion propagation for increased fe biodegradation. *Int J Bioprint*, 6:248. https://doi.org/10.18063/ijb.v6i1.248
20. Qian G, Fan P, He F, *et al*., 2019, Novel Strategy to Accelerate Bone Regeneration of Calcium Phosphate Cement by Incorporating 3D Plotted Poly (Lactic-co-glycolic Acid) Network and Bioactive Wollastonite. *Adv Healthc Mater*, 8:18013. https://doi.org/10.1002/adhm.201801325
21. Qian G, Lu T, Zhang J, *et al*., 2020, Promoting Bone Regeneration of Calcium Phosphate Cement by Addition of PLGA Microspheres and Zinc Silicate Via Synergistic Effect of *In-Situ* Pore Generation, Bioactive ion Stimulation and Macrophage Immunomodulation. *Appl Mater Today*, 19:100615. https://doi.org/10.1016/j.apmt.2020.100615
22. Yuan S, Chua CK, Zhou K, 2019, 3D-printed Mechanical Metamaterials with High Energy Absorption. *Adv Mater Technol*, 4:1800419. https://doi.org/10.1002/admt.201800419
23. Ng WL, Lee J M, Zhou M, *et al*., 2020, Vat Polymerization-based Bioprinting-Process, Materials, Applications and Regulatory Challenges. *Biofabrication*, 12:022001. https://doi.org/10.1088/1758-5090/ab6034
24. Ng WL, Chua CK, Shen YF, 2019, Print me an Organ! Why we are not there yet. *Prog Polym Sci*, 97:101145. https://doi.org/10.1016/j.progpolymsci.2019.101145
25. Alabort E, Barba D, Reed RC, 2019, Design of Metallic Bone by Additive Manufacturing. *Script Mater*, 164:110–14. https://doi.org/10.1016/j.scriptamat.2019.01.022
26. Shuai C, Li Y, Yang W, *et al*., 2020, Graphene Oxide Induces Ester Bonds Hydrolysis of Poly-l-lactic Acid Scaffold to Accelerate Degradation. *Int J Bioprint*, 6:249. https://doi.org/10.18063/ijb.v6i1.249
27. Liu J, Wei X, Wang X, *et al*., 2011, High-yield Synthesis of Ultrathin Silica-Based Nanosheets and their Superior Catalytic Activity in H_2O_2 Decomposition. *Chem Commun*, 47:6135–7. https://doi.org/10.1039/c1cc10280j
28. Hallab NJ, Bundy J, O'Connor K, *et al*., 2001, Evaluation of Metallic and Polymeric Biomaterial Surface Energy and Surface Roughness Characteristics for Directed Cell Adhesion. *Tissue Eng*, 7:55–71. https://doi.org/10.1089/107632700300003297
29. Ranjbar HA, Nourany M, Mollavali M, *et al*., 2020, Stimuli-responsive Polyurethane Bionanocomposites of Poly (ethylene glycol)/poly (ε-caprolactone) and [poly (ε-caprolactone)-grafted-] Cellulose Nanocrystals. *Polym Adv Technol*, 32:5062. https://doi.org/10.1002/pat.5062
30. Alnoor O, Laoui T, Ibrahim A, *et al*., 2020, Graphene Oxide-based Membranes for Water Purification Applications: Effect of Plasma Treatment on the Adhesion and Stability of the Synthesized Membranes. *Membranes*, 10:292. https://doi.org/10.3390/membranes10100292
31. Xin S, Gregory CA, Alge DL, 2020, Interplay between Degradability and Integrin Signaling on Mesenchymal Stem Cell Function within Poly (Ethylene Glycol) Based Microporous Annealed Particle Hydrogels. *Acta Biomater*, 101:227–36. https://doi.org/10.1016/j.actbio.2019.11.009
32. Yang L, Jiang Z, Zhou L, *et al*., 2017, Hydrophilic Cell-derived Extracellular Matrix as a Niche to Promote Adhesion and Differentiation of Neural Progenitor Cells. *RSC Adv*, 7:45587–94. https://doi.org/10.1039/c7ra08273h
33. Prochor P, Frossard L, Sajewicz E, 2020, Effect of the Material's Stiffness on Stress-shielding in Osseointegrated Implants for Bone-anchored Prostheses: A Numerical Analysis and Initial Benchmark Data. *Acta Bioeng Biomech*, 22:1–24. https://doi.org/10.37190/abb-01543-2020-02
34. Shuai C, Wang B, Bin S, *et al*., 2020, TiO_2-induced *In Situ* Reaction in Graphene Oxide-reinforced AZ61 Biocomposites to Enhance the Interfacial Bonding. *ACS Appl Mater Interf*, 12:23464–73. https://doi.org/10.1021/acsami.0c04020
35. Shuai C, Liu G, Yang Y, *et al*., 2020, A Strawberry-like Ag-decorated Barium Titanate Enhances Piezoelectric and Antibacterial Activities of Polymer Scaffold. *Nano Energy*, 2020:104825. https://doi.org/10.1016/j.nanoen.2020.104825

36. Murugan R, Ramakrishna S, 2005, Development of Nanocomposites for Bone Grafting. *Compos Sci Technol*, 65:2385–406.
37. Samuel SP, Li S, Mukherjee I, *et al*., 2009, Mechanical Properties of Experimental Dental Composites Containing a Combination of Mesoporous and Nonporous Spherical Silica as Fillers. *Dent Mater*, 25:296–301. https://doi.org/10.1016/j.dental.2008.07.012
38. Shuai C, Li S, Yang W, *et al*., 2020, MnO_2 Catalysis of Oxygen Reduction to Accelerate the Degradation of Fe-C Composites for Biomedical Applications. *Corros Sci*, 2020:108679. https://doi.org/10.1016/j.corsci.2020.108679
39. Shuai C, He C, Qian G, *et al*., 2020, Mechanically Driving Supersaturated Fe-Mg Solid Solution for Bone Implant: Preparation, Solubility and Degradation. *Compos Part B Eng*, 2020:108564. https://doi.org/10.1016/j.compositesb.2020.108564
40. Zou Z, Liu W, Cao L, *et al*., 2020, Advances in the Occurrence and Biotherapy of Osteoporosis. *Biochem Soc Trans*, 48:1623–36.
41. Heras C, Sanchez-Salcedo S, Lozano D, *et al*., 2019, Osteostatin Potentiates the Bioactivity of Mesoporous Glass Scaffolds Containing Zn^{2+} Ions in Human Mesenchymal Stem Cells. *Acta Biomater*, 89:359–371. https://doi.org/10.1016/j.actbio.2019.03.033
42. Wang B, Yang M, Liu L, *et al*., 2019. Osteogenic Potential of Zn^{2+}-passivated Carbon dots for bone Regeneration *In Vivo*. *Biomater Sci*, 7:5414–23. https://doi.org/10.1039/c9bm01181a
43. Kao YY, Chen YC, Cheng TJ, *et al*., 2012, Zinc Oxide Nanoparticles Interfere with Zinc Ion Homeostasis to Cause Cytotoxicity. *Toxicol Sci*, 125:462–72. https://doi.org/10.1093/toxsci/kfr319
44. Jin Z, Wu R, Shen J, *et al*., 2018, Nonstoichiometric Wollastonite Bioceramic Scaffolds with Core-shell Pore Struts and Adjustable Mechanical and Biodegradable Properties. *J Mech Behav Biomed Mater*, 88:140–9. https://doi.org/10.1016/j.jmbbm.2018.08.018
45. Zeng J, Xu L, Luo X, *et al*., 2021, A Novel Design of SiH/CeO_2 (111) van der Waals Type-II Heterojunction for Water Splitting. *Phys Chem Chem Phys*, 23:2812–8. https://doi.org/10.1039/d0cp05238h
46. Yu Y, Liu K, Wen Z, *et al*., 2020, Double-edged Effects and Mechanisms of Zn^{2+} Microenvironments on Osteogenic Activity of BMSCs: Osteogenic Differentiation or Apoptosis. *RSC Adv*, 10:14915–27. https://doi.org/10.1039/d0ra01465f
47. Zou A, Liang H, Jiao C, *et al*., 2020, Fabrication and Properties of $CaSiO_3/Sr_3(PO_4)_2$ Composite Scaffold Based on Extrusion Deposition. *Ceram Int*, 47:4783–92. https://doi.org/10.1016/j.ceramint.2020.10.048
48. Han P, Wu C, Xiao Y, 2013, The Effect of Silicate Ions on Proliferation, Osteogenic Differentiation and Cell Signalling Pathways (WNT and SHH) of Bone Marrow Stromal Cells. *Biomater Sci*, 1:379–92. https://doi.org/10.1039/c2bm00108j